Differential responses of primary auditory cortex in autistic spectrum disorder with auditory hypersensitivity

Junko Matsuzaki[a], Kuriko Kagitani-Shimono[a], Tetsu Goto[b,c], Wakako Sanefuji[d], Tomoka Yamamoto[d], Saeko Sakai[a], Hiroyuki Uchida[a], Masayuki Hirata[b], Ikuko Mohri[a], Shiro Yorifuji[c] and Masako Taniike[a]

The aim of this study was to investigate the differential responses of the primary auditory cortex to auditory stimuli in autistic spectrum disorder with or without auditory hypersensitivity. Auditory-evoked field values were obtained from 18 boys (nine with and nine without auditory hypersensitivity) with autistic spectrum disorder and 12 age-matched controls. Autistic disorder with hypersensitivity showed significantly more delayed M50/M100 peak latencies than autistic disorder without hypersensitivity or the control. M50 dipole moments in the hypersensitivity group were statistically larger than those in the other two groups. M50/M100 peak latencies were correlated with the severity of auditory hypersensitivity; furthermore, severe hypersensitivity induced more behavioral problems. This study indicates auditory hypersensitivity in autistic spectrum disorder as a characteristic response of the primary auditory cortex, possibly resulting from neurological immaturity or functional abnormalities in it. *NeuroReport* **23:113–118**

NeuroReport 2012, **23**:113–118

Keywords: auditory-evoked field, auditory hypersensitivity, autistic spectrum disorder, magnetoencephalography

[a]United Graduate School of Child Development, [b]Department of Neurosurgery, [c]Division of Function Diagnostic Sciences and [d]Department of Molecular Research Center for Children's Mental Development, Osaka University Graduate School of Medicine, Osaka, Japan

Correspondence to Kuriko Kagitani-Shimono, MD, PhD, United Graduate School of Child Development, Osaka University Graduate School of Medicine, Osaka, 2-2 Yamadaoka, Suita, Osaka 565-0871, Japan
Tel & Fax: +81 6 6879 3863;
e-mail: kuriko@ped.med.osaka-u.ac.jp

Received 21 September 2011 **accepted** 1 November 2011

Introduction

Autistic spectrum disorder is a neurodevelopmental disorder characterized by qualitative impairments in social interactions and communication skills, along with a restricted repetitive and stereotyped pattern of behavior [1]. In addition to these core features, the coincidence of sensory processing abnormalities in autistic disorder has been reported at a frequency of 42–88% [2,3]. Especially, auditory hypersensitivity is the most common sensory impairment, interrupting behavioral adaptation [4]. In earlier studies, many researchers found different auditory processing in autistic disorder compared with that in typically developing controls: the III–V interpeak latency of the auditory brainstem response was longer in autistic disorder than in control patients [5]. Event-related potentials and magnetoencephalography (MEG) studies also showed delayed responses to auditory stimuli in autistic disorder [6,7]. These electrophysiological studies showed auditory processing differences between autism and control. However, the physiological mechanism underlying auditory hypersensitivity has not been previously investigated. Therefore, the purpose of this study was to investigate the characteristic electrophysiological features in autistic spectrum disorder with auditory hypersensitivity. To clarify the difference in the response of the primary auditory cortex to auditory stimuli, we examined the auditory-evoked field and analyzed it in association with the characteristic traits of auditory hypersensitivity.

Methods

Participants

Eighteen male children with high-functioning autistic spectrum disorder (9.52 ± 1.72 years) and 12 age-matched male controls (10.08 ± 1.73 years) were recruited at the Osaka University Hospital (Table 1). The diagnosis of autistic spectrum disorder was made with reference to the *Diagnostic and Statistical Manual of Mental Disorders* (fourth edition)-Text Revision [1]. Furthermore, the diagnosis was confirmed by the Japanese version of Autism Screening Questionnaire (ASQ-J) [8,9] and the Autism Diagnostic Observation Schedule-Generic (ADOS-G) [10]. Intellectual quotient was assessed by using the *Wechsler Intelligence Scale for Children* (third version). In order to evaluate the characteristics of the auditory hypersensitivity and behavioral problems, we assessed the sensory profile (SP) [11] and used the Japanese version of the Child Behavior Checklist (CBCL) [12,13]. Children with autistic spectrum disorder were divided into two groups on the basis of the auditory item score of the SP: autistic disorder with auditory hypersensitivity and that without it. The cut-off value was set at 30. Controls were not only age-matched

0959-4965 © 2012 Wolters Kluwer Health | Lippincott Williams & Wilkins DOI: 10.1097/WNR.0b013e32834ebf44

Table 1 Demographic information

	Autistic disorder with auditory hypersensitivity ($N=9$)	Autistic disorder without auditory hypersensitivity ($N=9$)	Controls ($N=12$)
Items	Mean ± SD	Mean ± SD	Mean ± SD
Age (years)	9.64 ± 1.89	9.40 ± 1.64	10.08 ± 1.73
FIQ	102.17 ± 22.71	96.13 ± 8.18	–
ADOS-G	12.33 ± 2.45	12.75 ± 3.66	–
ASQ	15.33 ± 5.85*1	15.11 ± 4.05*2	2.83 ± 3.29*1, *2
SP Auditory Item Score	20.33 ± 5.56**1	31.78 ± 2.44**1	39.00 ± 1.41**1
CBCL	75.43 ± 18.15	51.63 ± 13.93	–

ADOS-G, Autism Diagnostic Observation Schedule-Generic (total score); ASQ, Autism Screening Questionnaire (cut-off ≥ 13) (*1, *2; $P<0.01$); CBCL, Child Behavior Checklist (total score); FIQ, full-scale intellectual quotient of *Wechsler Intelligence Scale for Children* (third version); SP, sensory profile, (**1; $P<0.01$).
*In ASQ, there are significant differences between autistic disorder with hypersensitivity and controls and also between autistic disorder without hypersensitivity and controls.
**In SP, there are significant differences between autistic disorder with hypersensitivity and autistic disorder without hypersensitivity and controls, and also between autistic disorder without hypersensitivity and controls.

children without a history of neurological diseases or developmental disorders, but also those who were not receiving special education services. In addition, all controls were assessed by the ASQ and SP, and showed no autism traits or sensory hypersensitivity. Written informed consent was obtained from the parents of all participants in the study, which was approved by the Institutional Review Board of Osaka University Hospital.

Auditory stimuli

Auditory stimuli, which were made by a presentation system (Yokogawa Electric Corporation, Kanazawa, Japan), were delivered through a sound pressure transducer and sound conduction tubing to the participant's auditory canal through ear tip inserts. A 1000-Hz sinusoidal tone pip of 200 ms duration was binaurally presented (with 10-ms rise and fall times). Stimuli were randomly presented with interstimulus intervals of 2700–3300 ms. The total number of stimuli was 100.

Measurements

Measurements by MEG were performed with the participants lying down on a bed in a magnetically shielded room using a 160-channel whole-head MEG system equipped with SQUID gradiometers (PQ1160C, Yokogawa Electric Corporation). Data were acquired at a sampling rate of 1000 Hz, with an online band-pass filter between 0.03 Hz and 200 Hz. The positions of five head marker coils were obtained before and after recording to evaluate head movement. Anatomical magnetic resonance imaging (MRI) data were obtained using a 3.0-T whole-body magnetic resonance scanner with a standard whole-head coil (Signa HDxt Excite 3.0 T, GE Healthcare UK Ltd, Buckinghamshire, UK).

In order to align MEG data with individual MRI data, we scanned the three-dimensional facial surface of each participant (FastSCAN Cobra, POLHEMUS, ARANZ Scanning Limited, Christchurch, New Zealand). Five head marker coils were attached to the scalp before recording the MEG, which provided the position and orientation of MEG sensors relative to the head. Three-dimensional facial surface data were superimposed on the anatomical facial surface provided by the MRI data.

Data analysis

The MEG data were analyzed at MEG Laboratory (Yokogawa Electric Corporation). The epochs were defined from 100 ms before stimulation to 1000 ms after stimulation. This prestimulus period of 100 ms was used as the baseline for the determination of ambient brain activity and noise of each epoch. Epochs containing artifacts such as eye blinks, head movements, and others were eliminated for each participant. The epochs were averaged for each condition [14], and averaged waveforms were high-pass filtered using a cut-off frequency of 3 Hz, low-pass filtered (cut-off frequency of 45 Hz), and band-pass filtered (cut-off frequency of 8–25 Hz). We evaluated the responses of each hemisphere by using half of all channels. To determine the M50/M100 peak, we calculated the root mean square of half of all channels. The M50/M100 peak was determined as the peak in the root mean square value in the intervals of 30–70 ms and 80–200 ms, respectively. The data were statistically examined by repeated-measures analysis of variance using PASW Statistics v. 18.0 (IBM, Tokyo, Japan), and the Pearson test was used to examine the correlation.

Results

Demography

The ASQ scores of autistic disorder with/without auditory hypersensitivity were significantly higher than those of the control (all $Ps < 0.01$). There was no significant group difference in age, scores of full intellectual quotient, ADOS-G, or CBCL between autistic disorder with auditory hypersensitivity and that without it (all $Ps > 0.15$). However, there was a significant difference in the auditory score of the SP between these two groups, between autistic disorder with auditory hypersensitivity and control and between autistic disorder without auditory hypersensitivity and the control (all $Ps < 0.01$). Autistic disorder with hypersensitivity showed a significantly lower auditory item score of the SP (20.33 ± 5.56)

than that without it (31.78 ± 2.44) or the control [39.00 ± 1.41; F (2, 27) = 76.34, $P < 0.01$; Table 1]. Furthermore, there was a statistically significant correlation between auditory item scores of the SP and the total scores of the CBCL ($r = -0.62$, $P < 0.05$; Fig. 1).

M50/M100 group differences

Auditory-evoked field waveform, magnetic isofield maps, and dipole sources were superimposed on the MRI of individual participants selected as an example from each of the three groups (Fig. 2).

Peak amplitude

There was no significant difference in the M50 peak amplitude between autistic disorder with auditory hypersensitivity (41.37 ± 11.46 fT/cm) and that without it (74.67 ± 33.67 fT/cm) or the control (53.54 ± 16.34 fT/cm), or in the M100 peak amplitude between autistic disorder with auditory hypersensitivity (57.44 ± 17.85 fT/cm) and that without it (61.74 ± 33.67 fT/cm) or the control (83.08 ± 16.34 fT/cm). Furthermore, there was no statistically significant correlation between SP and M50/M100 peak amplitude (all Ps > 0.15).

Peak latencies

M50 peak latencies were significantly longer in autistic disorder with auditory hypersensitivity than in the control [F (2, 27) = 4.35, $P < 0.05$; Fig. 3a]. However, autistic disorder with auditory hypersensitivity showed significantly longer M100 peak latencies than the other two groups [F (2, 27) = 12.59, $P < 0.01$; Fig. 3b]. There was a statistically significant negative correlation between auditory item scores of the sensory profile and M50 ($r = -0.52$, $P < 0.01$; Fig. 3c) or M100 latencies ($r = -0.69$, $P < 0.01$; Fig. 3d).

Dipole moments

The difference in dipole moments between autistic disorder with auditory hypersensitivity and the control was statistically significant [F (2, 24) = 3.75, $P < 0.05$], with the former showing larger M50 dipole moments (Fig. 3e). In addition, there was a statistically negative correlation between M50 dipole moment and auditory item scores of the SP ($r = -0.50$, $P < 0.05$; Fig. 3f). M100 dipole moments did not show any differences between groups (data not shown). There was no statistically significant correlation between the ASQ, CBCL or ADOS-G, and MEG measurements mentioned above (all Ps > 0.15).

Discussion

Many autistic spectrum disorders with auditory hypersensitivity tend to have impaired adaptation in their daily lives. Actually, in our study, SP auditory scores were significantly correlated with behavioral problems, as revealed by the CBCL scores.

Fig. 1

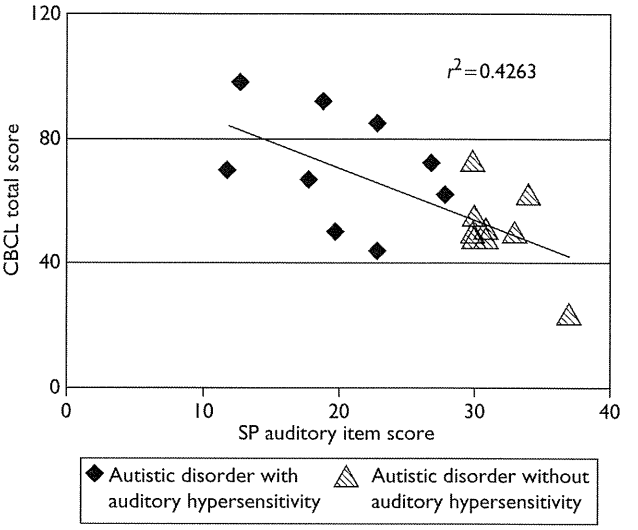

Scatter plot of the sensory profile (SP) auditory item scores and the child behavior checklist (CBCL). The total scores of the child behavior checklist were negatively correlated with auditory item scores of the SP (Pearson's test, $r = -0.62$, $P < 0.05$).

This study clearly demonstrated that M50/M100 latencies differed between autistic disorder with auditory hypersensitivity and that without it or the control group, and that auditory scores of the SP (i.e. severe hypersensitivity) were also significantly correlated with M50/M100 latencies (i.e. delayed latency) in autistic children. As there was no difference in the scores of the ASQ or the ADOS-G between autistic disorders with auditory hypersensitivity and that without it, auditory hypersensitivity might not be correlated with the severity of the core symptoms of autistic disorder, such as impaired social interaction.

Roberts *et al.* [7] reported that the peak latency of the primary auditory cortex is shortened with increasing age from 6 to 15 years in control, but not in autistic participants, and they speculated that the latter have maturational abnormalities in their auditory cortex. As the source of M50/M100 is generated from the primary auditory cortex, these findings suggest that a more severe auditory hypersensitivity corresponded to a more delayed response of the primary auditory cortex to auditory stimuli.

Gage *et al.* [15] and Bruneau *et al.* [16] reported longer latency in autistic children and hypothesized that this is due to abnormalities in myelination processes that would result in slower transmission rates in central auditory pathways.

Furthermore, in our study, the more severe auditory sensitivity was correlated with larger M50 dipole moments. The dipole moment has been used as a

Fig. 2

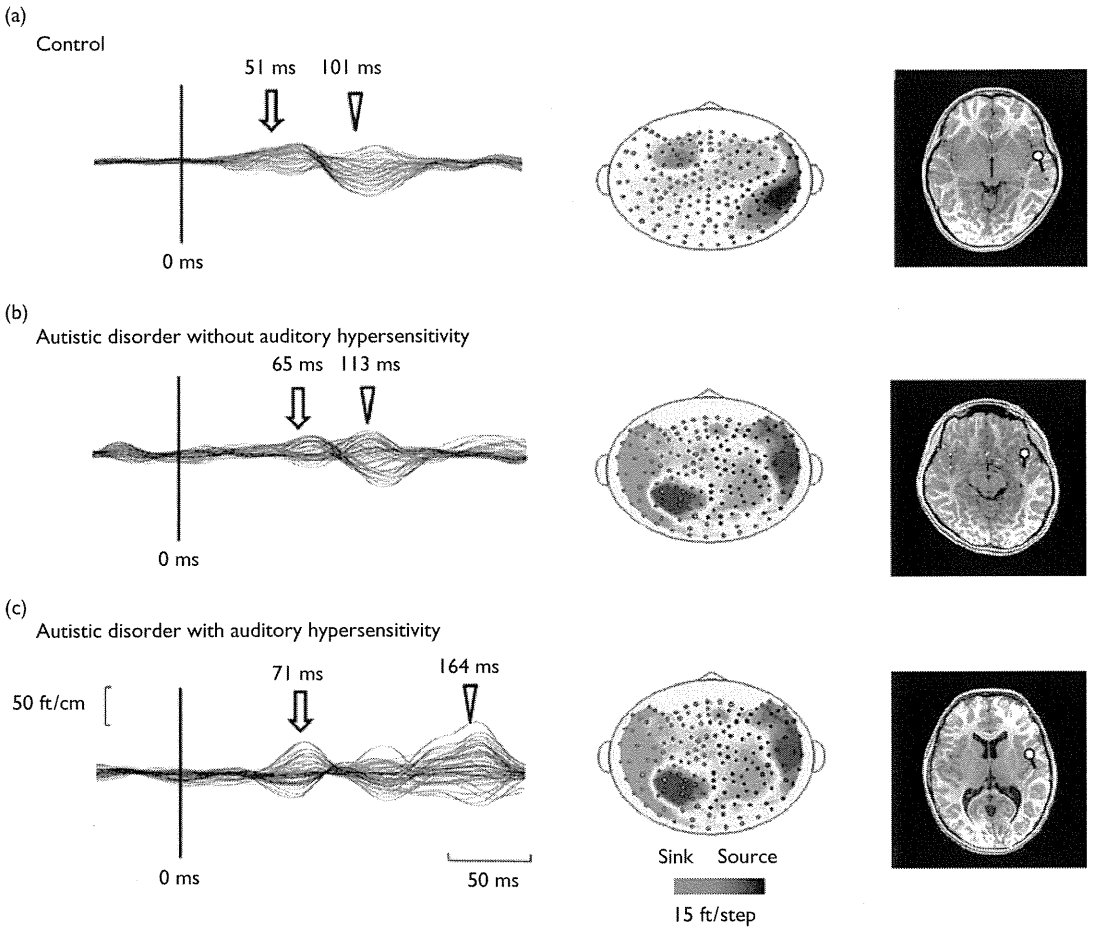

Representative figures of auditory-evoked field waveforms (left), magnetic isofield maps (middle), and dipole sources (right) superimposed on the individual brain magnetic resonance imaging of participants selected from each of the three groups. The magnetoisofield map shows the latency of M100 peak; and the dipole sources were estimated at the same time. (a) Controls, (b) autistic disorder without auditory hypersensitivity, and (c) autistic disorder with auditory hypersensitivity. Vertical lines in the left figures indicate stimulus onset (0 ms). Arrows and arrowheads indicate the M50 peak and the M100 peak, respectively. Both M50 and M100 latencies are longer in autistic disorder with auditory hypersensitivity than in the other two groups.

potential determinant of the absolute magnitude of neuronal activity [17,18]. Therefore, the increase in the M50 dipole moment may be explained by hyperactivity of the corresponding region of the primary auditory cortex.

In recent years, there have been findings of abnormal brain connectivity in autistic disorder [19], and additionally, autistic disorders from postmortem brains show disrupted minicolumns and decreased inhibitory interneurons [20]. Thus, abnormal brain connectivity resulting from reduced interneuron activity might induce cortical hypersensitivity in the primary auditory cortex. Various degrees of hypersensitivity could stem from interindividual heterogeneity in brain connectivity.

As another possibility, Guiraud *et al.* [21] reported that infants at high risk for autism show less habituation to repeated sounds than those at low risk. We speculated that this difference might be associated with auditory hypersensitivity in autism. In our study, we did not directly analyze this hypothesis. In a future study, the oddball paradigm of MEG may enable us to investigate whether the reduced habituation is associated with thalamic sensory gating.

These lines of evidence suggest that measurement of the auditory-evoked field could be an objective marker of auditory hypersensitivity as one of the autistic characteristics. This measurement would be especially useful for assessment of infants and nonverbal autistic disorder. As auditory hypersensitivity causes incomprehensible behavioral problems in daily life, earmuff usage or avoidance of noisy environments may be recommended for relief from discomforting sounds.

Fig. 3

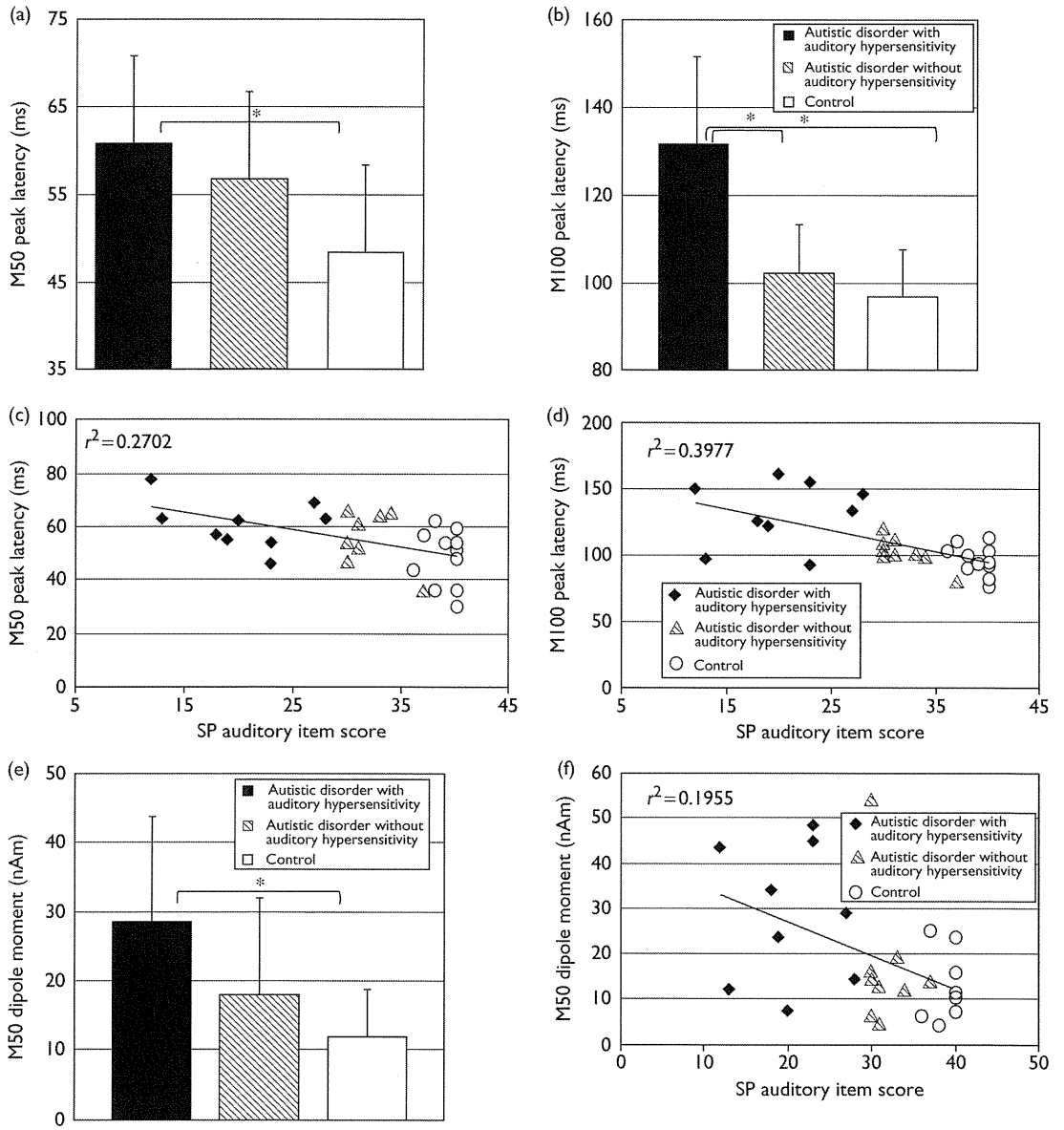

(a and b) Mean M50 and M100 peak latencies. Error bars represent one standard error of the mean. Both latencies in autistic disorder with auditory hypersensitivity are significantly longer than those in the control (*$P<0.05$). (c and d) Scatter plot of M50 peak latencies or M100 peak latencies and auditory item scores of sensory profile (SP). Both M50 and M100 peak latencies correlate negatively with auditory item scores of the SP ($r=-0.52$, $P<0.01$; $r=-0.69$, $P<0.01$). (e) Mean M50 dipole moment. Error bars represent one standard error of the mean. The M50 dipole moment in autistic disorder with auditory hypersensitivity is significantly larger than that in the control (*$P<0.05$). (f) Scatter plot of the M50 dipole moment and auditory item scores of the SP. There is a negative correlation between the two parameters ($r=-0.50$, $P<0.05$).

Conclusion

This study shows that M50/M100 responses generated by the primary auditory cortex were correlated with the severity of auditory hypersensitivity in children with autistic spectrum disorder. Understanding of the neurological basis of auditory hypersensitivity could have clinical benefits by providing an objective assessment of the severity of auditory hypersensitivity and by validating effective treatment for it in the future.

Acknowledgements

The authors are grateful to all participants and their parents.

We also thank Associate Professor Taku Hagiwara, Hokkaido University of Education, for the translated SP and permission to use it in our research. This study was supported by a Grant-in-aid for scientific research (No. 23591494) from the Ministry of Education, Culture, Sports, Science and Technology (MEXT).

Conflicts of interest

There are no conflicts of interest.

References

1 American Psychiatric Association. Diagnostic and Statistical Manual of Mental Disorders 4th Edition-Text Revision (DSM-IV-TR). Washington, DC: American Psychiatric Association; 2000.

2 Kientz MA, Dunn W. A comparison of the performance of children with and without autism on the sensory profile. *Am J Occup Ther* 1997; **51**:530–537.

3 Tomcheck SD, Dunn W. Sensory processing in children with and without autism: a comparative study using the short sensory profile. *Am J Occup Ther* 2007; **61**:190–200.

4 Lane AE, Young RL, Baker AEZ, Angley MT. Sensory processing subtypes in autism: association with adaptive behavior. *J Autism Dev Disord* 2010; **40**:112–122.

5 Rosenhall U, Nordin V, Brantberg K, Gillberg C. Autism and auditory brain stem responses. *Ear Hear* 2003; **24**:206–214.

6 Oram Cardy JE, Flagg EJ, Roberts W, Roberts TPL. Auditory evoked fields predict language ability and impairment in children. *Int J Psychophysiol* 2008; **68**:170–175.

7 Roberts TPL, Khan SY, Rey M, Monroe JF, Cannon K, Blaskey L, *et al.* MEG detection of delayed auditory evoked responses in autism spectrum disorders: towards an imaging biomarker for autism. *Autism Res* 2010; **3**:8–18.

8 Berument SK, Rutter M, Lord C, Pickles A, Bailey A. Autism screening questionnaire: diagnostic validity. *Br J Psychiatry* 1999; **175**:444–451.

9 Dairoku H, Senju A, Hayashi E, Tojo Y, Ichikawa H. Development of Japanese version of autism screening questionnaire. *Kokuritsu Tokushu Kyoiku Kenkyusho Ippan Kenkyu Houkokusho* 2004; **7**:19–34.

10 Di Lavore PC, Lord C, Rutter M. The pre-linguistic autism diagnostic observation schedule. *J Autism Dev Disord* 1995; **25**:355–379.

11 Dunn W. *Infant/Toddler Sensory Profile.* San Antonio, TX: Psychological Corporation; 2002.

12 Itani T, Kanbayashi Y, Nakata Y, Kita M, Fujii H, Kuramoto H, *et al.* Standardization of the Japanese version of the child behavior checklist/4–18. *Psychiatra et Neurologia Pediatrica Japonica* 2001; **41**:243–252.

13 Achenbach TM. *Manual for the child behavior checklist/4–18 and profile.* Burlington, VT: University of Vermont; 1991.

14 Gage NM, Siegal B, Callen M, Roberts TPL. Cortical sound processing in children with autism disorder: an MEG investigation. *Neuroreport* 2003; **14**:2047–2051.

15 Gage NM, Siegel B, Roberts TPL. Cortical auditory system maturational abnormalities in children with autism disorder: an MEG investigation. *Brain Res Dev Res* 2003; **144**:201–209.

16 Bruneau N, Roux S, Adirien JL, Barthelemy C. Auditory associative cortex dysfunction in children with autism: evidence from late auditory evoked potentials (N1 wave–T complex). *Clin Neurophysiol* 1999; **110**:1927–1934.

17 Okada Y. *Biomagnetism: neurogenesis of evoked magnetic fields.* New York: Plenum Press. 1983; pp. 399–408.

18 Tsutada T, Tsuyuguchi N, Hattori H, Shimada H, Shimogawara M, Kuramoto T, *et al.* Determining the appropriate stimulus intensity for studying the dipole moment in somatosensory evoked fields: a preliminary study. *Clin Neurophysiol* 1999; **110**:2127–2130.

19 Wass S. Distortions and disconnections: disrupted brain connectivity in autism. *Brain Cogn* 2011; **75**:18–28.

20 Casanova MF, Buxhoeveden DP, Switala AE, Roy E. Minicolumnar pathology in autism. *Neurology* 2002; **58**:428–432.

21 Guiraud JA, Kushnerenko E, Tomalski P, Davies K, Ribeiro H, Johnson MH, *et al.* Differential habituation to repeated sounds in infants at high risk for autism. *Neuroreport* 2011; **22**:845–849.

J Neurosurg 114:1715–1722, 2011

Real-time control of a prosthetic hand using human electrocorticography signals

Technical note

Takufumi Yanagisawa, M.D., Ph.D.,[1,2] Masayuki Hirata, M.D., Ph.D.,[1] Youichi Saitoh, M.D., Ph.D.,[1] Tetsu Goto, M.D., Ph.D.,[1] Haruhiko Kishima, M.D., Ph.D.,[1] Ryohei Fukuma, M.S.,[2,3] Hiroshi Yokoi, Ph.D.,[4] Yukiyasu Kamitani, Ph.D.,[2,3] and Toshiki Yoshimine, M.D., Ph.D.[1]

[1]Department of Neurosurgery, Osaka University Medical School, Osaka; [2]ATR Computational Neuroscience Laboratories, Kyoto; [3]Nara Institute of Science and Technology; and [4]Department of Precision Engineering, University of Tokyo, Japan

Object. A brain-machine interface (BMI) offers patients with severe motor disabilities greater independence by controlling external devices such as prosthetic arms. Among the available signal sources for the BMI, electrocorticography (ECoG) provides a clinically feasible signal with long-term stability and low clinical risk. Although ECoG signals have been used to infer arm movements, no study has examined its use to control a prosthetic arm in real time. The authors present an integrated BMI system for the control of a prosthetic hand using ECoG signals in a patient who had suffered a stroke. This system used the power modulations of the ECoG signal that are characteristic during movements of the patient's hand and enabled control of the prosthetic hand with movements that mimicked the patient's hand movements.

Methods. A poststroke patient with subdural electrodes placed over his sensorimotor cortex performed 3 types of simple hand movements following a sound cue (calibration period). Time-frequency analysis was performed with the ECoG signals to select 3 frequency bands (1–8, 25–40, and 80–150 Hz) that revealed characteristic power modulation during the movements. Using these selected features, 2 classifiers (decoders) were trained to predict the movement state—that is, whether the patient was moving his hand or not—and the movement type based on a linear support vector machine. The decoding accuracy was compared among the 3 frequency bands to identify the most informative features. With the trained decoders, novel ECoG signals were decoded online while the patient performed the same task without cues (free-run period). According to the results of the real-time decoding, the prosthetic hand mimicked the patient's hand movements.

Results. Offline cross-validation analysis of the ECoG data measured during the calibration period revealed that the state and movement type of the patient's hand were predicted with an accuracy of 79.6% (chance 50%) and 68.3% (chance 33.3%), respectively. Using the trained decoders, the onset of the hand movement was detected within 0.37 ± 0.29 seconds of the actual movement. At the detected onset timing, the type of movement was inferred with an accuracy of 69.2%. In the free-run period, the patient's hand movements were faithfully mimicked by the prosthetic hand in real time.

Conclusions. The present integrated BMI system successfully decoded the hand movements of a poststroke patient and controlled a prosthetic hand in real time. This success paves the way for the restoration of the patient's motor function using a prosthetic arm controlled by a BMI using ECoG signals. *(DOI: 10.3171/2011.1.JNS101421)*

Key Words • brain-machine interface • prosthetic hand • electrocorticography signal • real time • support vector machine

There are several diseases and conditions that lead to a loss of muscle control without disruption of the patients' cognitive abilities. These include amyotrophic lateral sclerosis, brainstem stroke, spinal cord injury, muscular dystrophy, and cerebral palsy. Brain-machine interface technology can offer these patients greater independence and a higher quality of life, providing the individual with control of external devices with which to communicate with others and manipulate their environment according to their will.[29]

Several signal platforms could be used as input signals for BMIs in a clinical setting: EEG,[30] MEG,[27] neuronal ensemble activity recorded intracortically (single units)[8,9,28] and/or local field potentials,[1,15] and ECoG.[14,18,21] Each type of signal has proven to be useful for BMIs, although each has advantages and disadvantages regarding utility in an applied setting. Although EEG and MEG

Abbreviations used in this paper: BMI = brain-machine interface; ECoG = electrocorticography; EEG = electroencephalography; EMG = electromyography; FFT = fast Fourier transform; MEG = magnetoencephalography; SVM = support vector machine.

signals can be measured noninvasively,[30] they have low spatial resolution compared with the other signals and are susceptible to artifacts from other sources.[7] Single-unit recordings have been shown to convey large amounts of information for the successful control of a prosthetic arm in a self-feeding task of monkeys.[26] This type of BMI system has already been applied to paralyzed patients,[9] but the clinical implementation of intracortical BMIs is currently impeded by difficulty in maintaining stable long-term recordings and the substantial technical requirements of the recordings.[6,22] Electrocorticography has a higher spatial resolution and better signal-to-noise ratio than EEG or MEG. Its signals have been used to control the movement of a cursor on a computer screen,[21] to reconstruct the trajectory of a 2D arm movement,[18] and to decode a single finger movement.[16] Moreover, ECoG recordings have superior long-term stability than intracortical single-unit recordings, as well as lower technical difficulty and clinical risk.[4] Even though ECoG signals have been shown to be useful for BMI systems, they have not been used to control the movement of a prosthetic hand. Here, we propose an integrated BMI system to control the movement of a prosthetic hand using ECoG signals generated while the patient moved his hand.

Previously, we developed a system in which a patient's EMG signals were used to control the movement of a prosthetic hand.[12,17] This system records the EMG signals and converts them into a power spectrum to classify some simple movements. The user can control the prosthetic hand by performing or attempting to perform simple hand movements, such as hand grasping, hand opening, and making a scissor shape. By combining such simple movements, an amputee was able to use the prosthetic hand for writing by holding a pen, cooking by grasping a kitchen knife, and other activities of daily living.[32] In the present study, we removed the EMG sensors and control unit from this system and attached a new unit that records and classifies ECoG signals to control the prosthetic hand. The new integrated system was designed to classify some simple movements using only 3 frequency power bands of the ECoG signals.

With the new integrated system, the ECoG signals of a stroke patient were recorded when he performed 3 types of hand movements. Time-frequency analysis of the signals demonstrated that 3 frequency power bands contained the characteristic features relating to the movements. With these features, the state and the type of movement were inferred by 2 decoders. The decoding accuracy was compared among the 3 frequency bands to identify the most informative band. With the 2 decoders, the freely performed movements were inferred so that the prosthetic hand faithfully mimicked the individual's hand in real time.

Methods

Patient

This 64-year-old man with thalamic pain on the left side of his body participated in this study. He had incomplete left hemiparesis due to a right thalamic hemorrhage 7 years earlier. He was barely able to perform simple hand movements (grasping, opening, and making a scissor shape). Subdural electrodes had been implanted on the right sensorimotor cortex to reduce intractable pain by delivering electrical stimulation.[10] First, 2 sheets of a 30-electrode array were temporarily implanted on a broad cortical area around his hand motor strip to determine an optimal stimulation site where the maximum reduction of his pain was achieved. The number and location of the electrodes were chosen to stimulate the cortical area corresponding to the body parts with pain. These electrodes were implanted for 2 weeks. Then, after the optimal site was determined, an array of 4 electrodes was implanted at the optimal site for chronic stimulation to reduce the pain. The patient participated in our study during the 2 weeks of temporary electrode placement. He was informed of the purpose and possible consequences of this study, and written informed consent was obtained. The ethics committee of Osaka University Hospital approved the present study.

Prosthetic Hand

The prosthetic hand was an experimental anthropomorphic hand developed by Dr. Yokoi.[12] The general movement mechanisms and degrees of freedom of the hand mimicked those of a human hand. The hand was equipped with 8 DC motors to independently actuate 8 individual tendons of the hand. The 8 tendons work in a coordinated manner to accomplish flexion or extension of each individual finger. The commands to the hand were updated by the host computer system every 200 msec.

Recording Methods

Sixty planar-surface platinum grid electrodes (2 sheets of a 5 × 6 array, Unique Medical Co.) were placed over the patient's right sensorimotor cortex (see Fig. 2A). The electrodes had a diameter of 3 mm and a center-to-center interelectrode distance of 7 mm. Video recording was performed during experiments. Electromyography recordings of the contralateral flexor digitorum superficialis muscle were collected at the same time. The video and EMG recordings were not used for the decoding but were used to identify the onset of the actual movement during offline analysis.

The location of the implanted electrodes was identified by standard neurosurgical techniques, both anatomically and electrophysiologically. After induction of general anesthesia, we performed a frontoparietal craniotomy over the sensorimotor cortex. The location of the central sulcus was estimated using preoperative MR imaging and confirmed by the phase reversal of the N20 component of the intraoperative somatosensory evoked potentials.

Movement Tasks

Experiments were performed in an electromagnetically shielded room approximately 1 week after electrode placement. The patient was instructed to perform 3 types of movements with his left hand: a grasping motion, a hand-opening motion, and a scissor-shape motion (extension of the second and third fingers). He selected and

performed 1 of the 3 hand movements immediately after the presentation of a sound cue that recurred every 5.5 seconds (calibration period [Fig. 1A]). The sound cue was delivered from a loudspeaker controlled by Matlab 2007b (Mathworks), consisting of 3 beeps presented every 1 second. The patient was instructed to move his hand just after the third sound and to return his hand to a resting position immediately after the movement. For the resting position, the patient was instructed to relax his hand while slightly flexing his fingers. The 3 types of movement were performed approximately 40 times each. This calibration period took approximately 20 minutes with some breaks in between. During this period, there was no training of the patient.

After the calibration period with the external cues, the patient performed the same task at self-paced intervals without any external cues (free-run session [Fig. 1B]). The free-run session lasted for approximately 20 minutes with some breaks. Therefore, all of the experiments in this study took only approximately 1 hour. Notably, the patient performed the free-run task without training to control the prosthetic hand; indeed, it was only necessary to train the decoder to the ECoG signals obtained in the calibration period (see the *Decoding Algorithms* section for details).

Data Collection and Preprocessing

Electrocorticography signals were measured using a 128-channel digital EEG system (EEG 2000, Nihon Koden Corp.) and digitized at a sampling rate of 1000 Hz. All subdural electrodes were referenced to a scalp electrode placed on the nasion. The bandpass filter for the data analysis was set to 0.16–300 Hz.

At first, during the calibration period, the ECoG signals of all implanted electrodes were examined for 4000 msec in each session (–2000 to 2000 msec from the cue onset of each movement). A time-frequency analysis of the ECoG signals was performed using EEGLAB v5.03.[5] The power spectrum of the ECoG signals was analyzed for each electrode and each type of movement. From the results of the power spectrum, we identified 3 frequency power bands with characteristic modulation during the movement tasks: 1–8, 25–40, and 80–150 Hz

For the decoding analysis, the ECoG signals of all implanted electrodes were obtained by reference to the 3 beeps. Figure 1A shows the duration of the ECoG signals used for the decoding analysis: "N," ECoG signals of 1 second after the first sound; "R," ECoG signals of 1 second after the second sound; and "M," ECoG signals of 1 second after the third sound. An FFT algorithm was performed for each 1-second signal to obtain the 3 frequency power bands (1–8, 25–40, and 80–150 Hz). The FFT was performed using EEGLAB v5.03. For each trial and electrode, the R and M frequency power bands were normalized by dividing them with the corresponding power of N. The normalized M and R power bands were used as the input features for the following decoding analysis (Fig. 1A).

In the free-run session, the 1-second ECoG signals were recorded online every 200 msec. The FFT algorithm was performed for each 1-second signal to obtain the 3 frequency power bands for each electrode. The frequency power bands of each electrode were divided by the corresponding power bands of the baseline features (baseline features were defined as the mean frequency power bands of N that were obtained by averaging the features of N for all trials in the calibration period).

Decoding Algorithms

With the features obtained in the calibration period, we constructed 2 decoders, or linear classifiers, to infer the patient's movements on a trial-by-trial basis. The decoders were trained or calculated using mathematical algorithms to infer the patient's movements using only a novel ECoG signal. The normalized powers of the 3 frequency bands (features) were used to train the 2 decoders based on the linear SVM.[31] Decoder 1 was trained to classify the movement state R or M, with the features of R and M (Fig. 1A). Decoder 2 was trained to predict the types of performed movement with the features of M (Fig. 1A). The mathematical details of these decoders are described in the supplementary section and the following references (http://www.cns.atr.jp/dni/en/downloads/brain-decoder-toolbox).[11,31]

The decoding accuracy was compared among the decoding of each of the 3 frequency bands to identify the most informative frequency band. The decoding accuracy was estimated by using a 5-fold cross-validation method *(Appendix)*.

Real-Time Decoding and Prosthetic Hand Control

The 2 decoders trained by the ECoG signals with the external cues were applied to the novel ECoG signals in real time. Decoder 1 classified the ECoG signals as either R or M to infer the onset of movement. When the inferred state changed from R to the two successive M decoder results, movement onset was inferred (or defined) as the time between R and M. Then, Decoder 2 classified the type of movement using the feature of the second M (Fig. 1B).

According to the decoding results, the prosthetic hand was controlled to mimic the patient's movements. When the decoding result from Decoder 1 was R, the prosthetic hand was moved to the predefined resting position. When movement onset was inferred by Decoder 1, then Decoder 2 inferred the type of movement using the current ECoG signals. Then, the prosthetic hand was moved to the predefined posture of the inferred movement. The posture was maintained for 1 second, regardless of the decoding results from Decoder 1. After 1 second, the prosthetic hand was moved back to the resting position.

Results

Offline Time-Frequency Analysis

During the movements in the calibration period, the power spectrum of the ECoG signals on the sensorimotor cortex varied consistently. Figure 2B illustrates an example of the power spectrum time locked to the external sound cue during the grasping movement. The signal was recorded from an electrode on the primary motor cortex

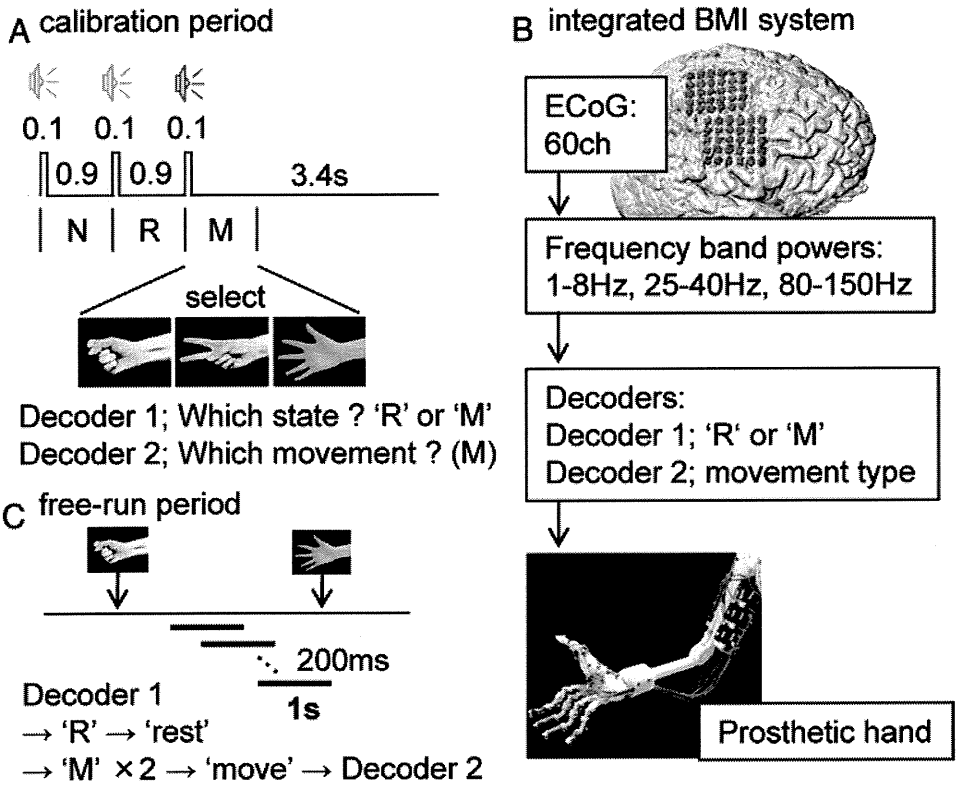

Fig. 1. Illustrations of the task and the integrated real-time decoding system. **A:** The task in the calibration period. The 1-second ECoG signals after each sound were defined as: 1st, "N" for normalization; 2nd, "R" for resting state; and 3rd, "M" for moving state. Decoders 1 and 2 were trained with the R + M and M ECoG signals, respectively. The representative photographs of hands show the task movements performed by a healthy individual. **B:** The task in the free-run period. The 1-second ECoG signals obtained every 200 msec were classified by Decoders 1 and 2 when the patient performed 1 of the 3 hand movements with arbitrary timing. **C:** Illustration of the integrated BMI system.

indicated by a blue arrow in Fig. 2A. As shown in Fig. 2B, the power reduction of the beta band (25–40 Hz) (event-related desynchronization) and the power increase of the theta (1–8 Hz) and gamma (80–150 Hz) bands (event-related synchronization) were observed around the movement onset. These frequency features, event-related desynchronization and event-related synchronization, were observed consistently on the sensorimotor cortex during the movement task.

The spatial distribution of these features on the electrodes differed depending on the movement (Fig. 2C). The increase in the power of the gamma and theta bands was observed at the localized area of the primary motor cortex. However, the decrease in the power of the beta band was observed diffusely around the primary motor cortex (Fig. 2C). The spatial distribution of each frequency power band differed among the 3 types of movement, especially for the gamma and theta bands. We selected these 3 frequency power bands as the input features for decoding.

Offline Analysis of Decoding

The patient's hand movement was inferred by the decoders using the frequency features of the ECoG signals on a trial-by-trial basis. Offline cross-validation analysis of the ECoG data measured during the calibration period revealed that the patient's state and the movement type were predicted with an accuracy of 79.6% (chance 50%) and 68.3% (chance 33.3%), respectively (Fig. 3). Among the 3 frequency bands, the gamma band power exhibited the best performance for the decoding of both the states and types of movement (Fig. 3).

Next, the trained Decoder 1 was tested to determine whether it could detect the onset of movement on a trial-by-trial basis. For the calibration period, the 1-second ECoG signals were classified using Decoder 1 for every 200 msec from –2 to 2 seconds relative to the onset cue. As shown in Fig. 4 left, the inferred rate of M was low before the onset cue and high after the cue. When we defined the onset as the time Decoder 1 inferred 2 successive M results after R, the movement onset was frequently inferred just after the actual onset cue (Fig. 4 right). Notably, 88% of the inferred onsets of movement were distributed between –0.5 to 0.5 seconds from the actual onset of the cue. For the calibration period, the movement onset was accurately inferred by the trained Decoder 1.

Real-Time Prosthetic Hand Control

Using the trained decoders, the ECoG signals were decoded in real time when the patient performed the 3 types of hand movement at an arbitrary timing (free-run period). Decoder 1 detected 61.0% of the movement onsets within 1 second from the actual onset of movement detected by the EMG signals. The mean difference be-

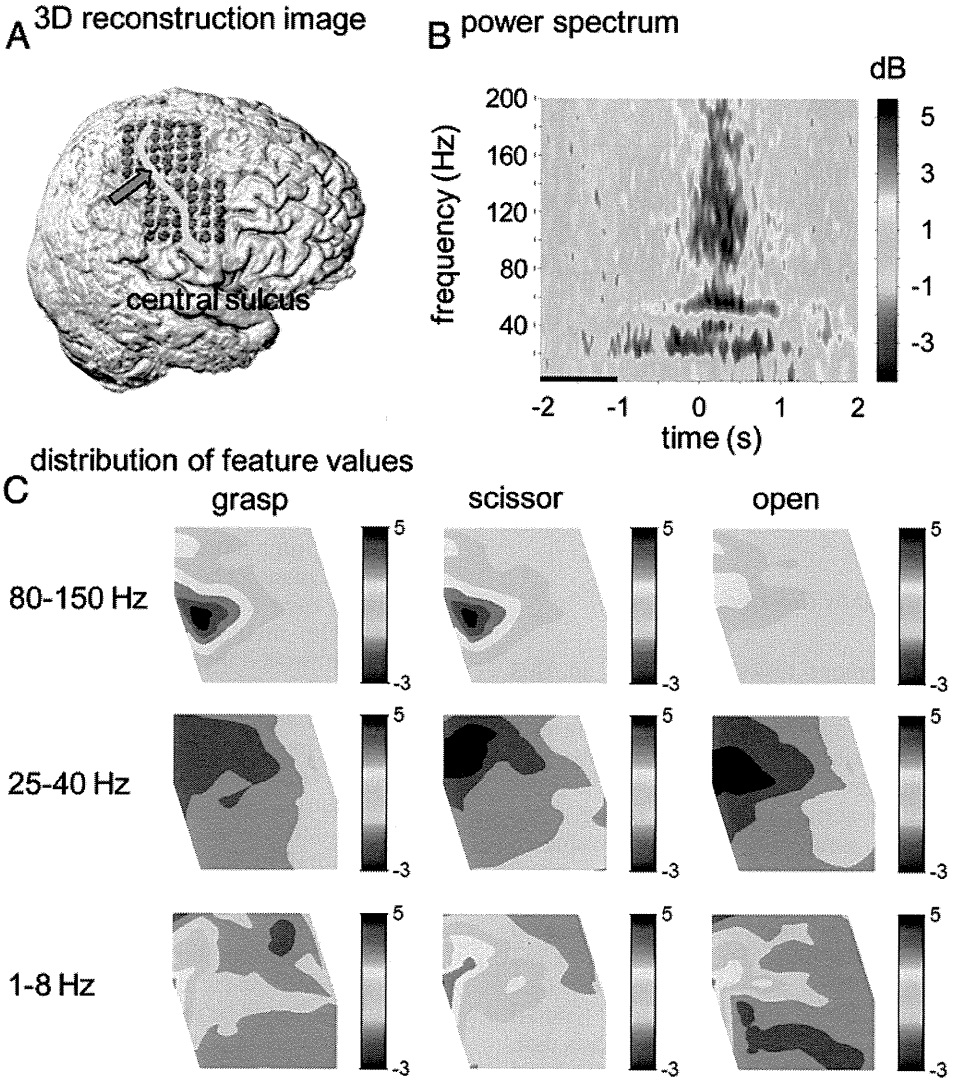

Fig. 2. Power spectrum of the ECoG signals during movement. **A:** Reconstructed MR image of the patient's brain with superimposed *red circles* indicating the position of the 60-channel grid electrodes. The *yellow line* indicates the location of the central sulcus. **B:** A power spectrum time locked to the external cues (Time 0 corresponds to the onset cue). The signals of the primary motor cortex (indicated by the *blue arrow* in **A**) were obtained during the grasping task. The *horizontal black line* shows the normalization period. **C:** Contour map of the mean frequency power bands. For each frequency band and each type of movement, the normalized power at 1 second after the onset of movement was averaged and shown on the location of the electrodes. The alignment of the electrode is the same as in panel **A**.

tween the inferred onset and the actual onset of movement was 0.37 ± 0.29 msec (± SD). The majority of the patient's hand movements were detected before the actual onset of movement (Fig. 5 left). However, the actual onset of movement of the prosthetic hand was delayed from the inferred onset timing due to the processing time (Video 1).

Video 1. A prosthetic hand (with a white glove) mimicking the patient's hand movements. The *markers* on the patient's arm were not used in the present study. Click here to view with Windows Media Player. Click here to view with Quicktime.

At the detected time, the type of movement was correctly decoded with an accuracy of 69.2%. The patient's hand movements inferred by the 2 decoders were performed by a prosthetic hand in real time (Fig. 5 right). Notably, the patient was not trained to control the prosthetic hand. The prosthetic hand was successfully controlled to faithfully mimic the patient's hand movements using only the ECoG signals without any external cues.

Discussion

We have demonstrated that a BMI system using ECoG signals can accurately reproduce a patient's hand movements without training the patient. The system learned the features of the ECoG signals, while the post-stroke patient moved his hand naturally following sound cues. The real-time decoding of ECoG signals was then successfully performed for movements without any external cues. This is the first report describing the control of a prosthetic hand in real-time using a BMI system with ECoG signals. These successful results with a post-

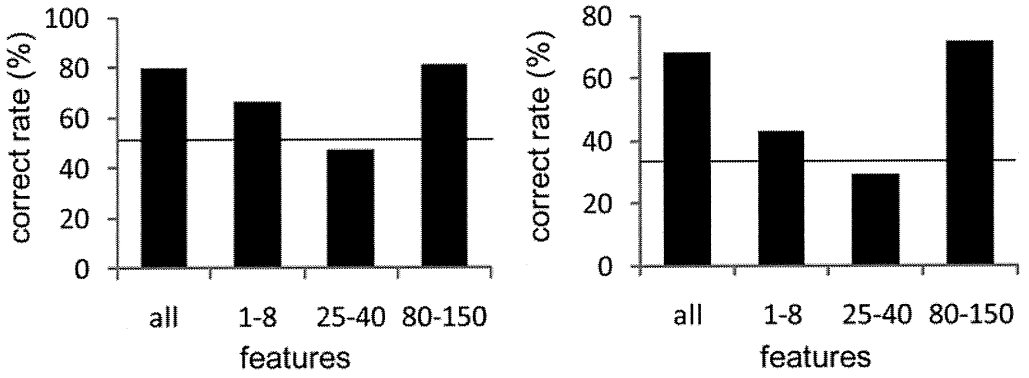

Fig. 3. Classification accuracy of the calibration period. The classification accuracy of the movement state **(left)** and the movement type **(right)** in the calibration period. The accuracy of the 3 frequency bands *(all)* and each single frequency band (1–8, 25–40, and 80–150 Hz) were compared. The *horizontal lines* show the chance level for each classification.

stroke patient indicate the feasibility of the clinical use of ECoG-based BMI.

Control of Prosthetic Hand by Classifying Simple Movements

Although the movement tasks performed in this study were simple compared with those in previous studies,[16,26] the success of our approach suggests a new way to restore the motor function of paralyzed patients. The combination of simple movements generated by the prosthetic hand is useful for activities of daily living.[32] For example, by classifying some simple hand movements with EMG signals, an amputee was able to use a prosthetic hand to improve her quality of life. This method of prosthetic control with simple movements may also be useful for controlling the prosthetic hand with ECoG signals. In addition, it has been shown that most variance in human hand postures can be accounted for by a small number of combined joint movements.[23] This means that, by combining some basic movements, a prosthetic hand could emulate most of the natural postures of a human hand. The control of a prosthetic device, by classifying some simple movements, with ECoG signals will enable a prosthetic hand to be a practical and useful device in a patient's day-to-day life.

Furthermore, ECoG signals have the potential to be decoded to infer more sophisticated movements such as playing the piano. The ECoG signals of epilepsy patients have been used to decode the movements of individual fingers.[16] Our method of controlling the prosthetic hand may be improved by using ECoG signals obtained in patients without motor dysfunction. In addition, the implantation of a high-density electrode array in the central sulcus may increase the information derived from ECoG signals. It is necessary to improve ECoG-based BMIs not only to adjust the control of a prosthetic device for activities of daily living but also to improve the ability to decode human motor representations.

Prosthetic Control by Paralyzed Patients

The clinical candidates for the BMI system are patients without muscle control of their limbs. Therefore, our method should be applicable in patients with complete paralysis. Previously, we showed that ECoG signals could be neurally decoded in patients with monoplegia.[31] Electrocorticography signals from the sensorimotor cortex in patients with brachial plexus avulsion were successfully decoded when the patients only intended or attempted to move their completely paralyzed upper limbs. The intention of movement was inferred accurately by a decoder

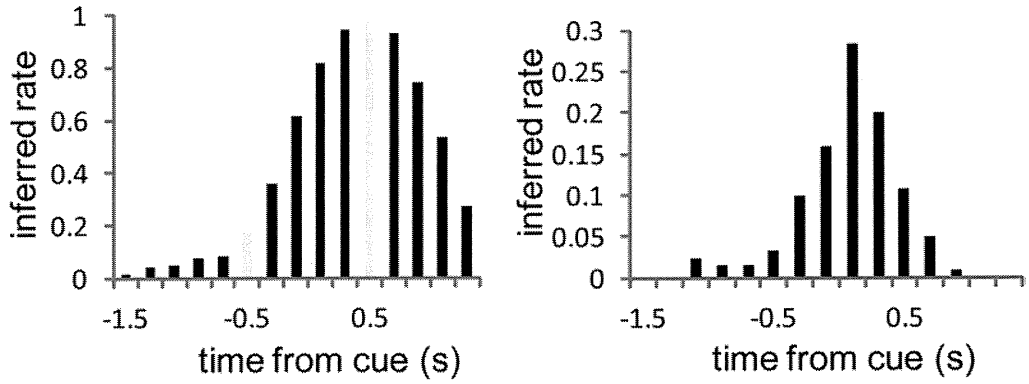

Fig. 4. Left: Onset timing inferred by Decoder 1 for the calibration period. The rate of M inferred by Decoder 1 using the 1-second ECoG signals sliding by 200 msec from –2 to 2 seconds. The horizontal axis shows the middle time of the 1-s ECoG signal (Time 0 corresponds to the onset cue). The *gray bars* correspond to the training data sets of Decoder 1. **Right:** The rate of onset inferred by Decoder 1.

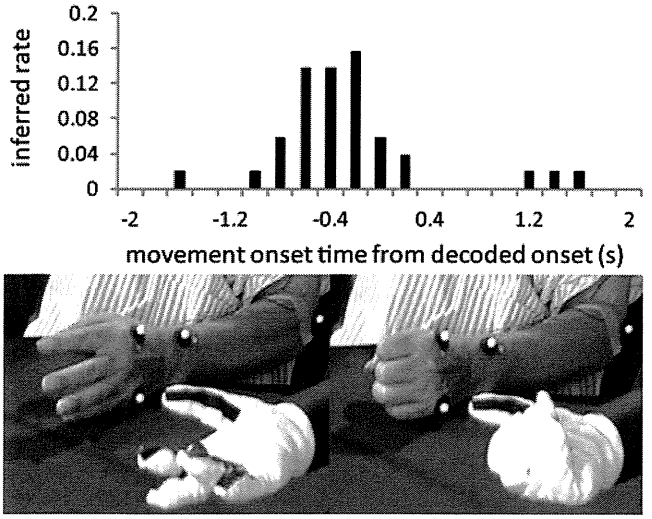

FIG. 5. Real-time decoding and prosthetic hand control with ECoG. **A:** The distribution of the actual movement onset timing from the nearest inferred onset timing by Decoder 1 (free-run period). **B:** Representative photographs of the prosthetic hand (with a white glove) controlled by the poststroke patient's ECoG signals in real time. A prosthetic hand (with a white glove) mimicked the patient's hand movements. The *markers* on the patient's arm were not used in the present study.

trained by the same method used in the present study. By using simple and common movements that can be easily planned by patients, our method may be applicable to a large number of paralyzed patients as a clinically beneficial device to restore their motor functions.

Usefulness of ECoG Signals From the Gamma Band Power

Decoding analysis of the ECoG signals revealed that the gamma band power was the most informative in inferring the state and type of hand movement among the 3 frequency bands. This result was consistent with previous studies in which human movements were inferred using ECoGs.[18,21] Moreover, the power increase of the gamma band correlates with the firing activities of neurons representing neural information.[19,20] Thus, the information contained within the gamma band facilitates the use of ECoG signals in a clinically applicable BMI system.

Among the currently available signal platforms for BMI, intracortical recordings have been shown to provide the largest amount of information to decode movements by using the firing activities of neurons.[24,26] However, this method is associated with difficulties in maintaining stable long-term signals and substantial technical difficulties in recording the signals. Therefore, clinical application of these signals is impeded.[13] Electrocorticography signals are superior to intracortical signals with respect to stability and durability, as demonstrated in monkeys over a 1-year period.[4] On the other hand, with noninvasive signal platforms, such as EEG and MEG, it is difficult to record the gamma band power on a trial-by-trial basis.[27] With ECoG, the gamma band power is consistently available to infer movements on a trial-by-trial basis and may be recorded for a much longer time than intracortical recordings. Therefore, although ECoG is an invasive recording technique, it provides a promising signal that could be used for a BMI in the clinical setting.

Conclusions

The real-time decoding of the ECoG signal using the gamma band power was applied successfully to allow a paralyzed patient to control a prosthetic hand. This success may lead to the development of a clinically feasible BMI system that uses the safe and stable ECoG signals. Our method of using the combination of simple movements paves the way for the restoration of motor function in paralyzed patients using a prosthetic arm controlled by a BMI through ECoG signals.

Disclosure

This work was supported in part by the Strategic Research Program for Brain Sciences of MEXT, Grants-in-Aid for Scientific Research (no. 22700435) from JSPS, Nissan Science Foundation, the Ministry of Health, Labor and Welfare (no. 18261201), and the SCOPE, SOUMU.

Author contributions to the study and manuscript preparation include the following. Conception and design: Hirata, Yanagisawa, Kamitani. Acquisition of data: Hirata, Yanagisawa, Goto, Fukuma. Analysis and interpretation of data: Hirata, Yanagisawa, Kamitani. Drafting the article: Yanagisawa. Critically revising the article: Hirata. Reviewed final version of the manuscript and approved it for submission: all authors. Statistical analysis: Yanagisawa. Administrative/technical/material support: Hirata, Saitoh, Goto, Kishima, Fukuma, Yokoi, Kamitani, Yoshimine. Study supervision: Hirata, Kamitani, Yoshimine.

Appendix

Construction of the Decoders

The decoder is a mathematical algorithm used to calculate a linearly weighted sum of the features $x = (x_1, x_2, \cdots, x_N)$ plus a bias for each class of movement ("linear detector function," $g_{class}(x)$). In the equation, x_i corresponds to the *i*-th feature of N features, $w_{i,class}$ is the weight of the *i*-th feature, and $w_{0,class}$ is the bias. Here, each feature corresponds to a certain frequency band power for each electrode. That is, 3 (frequency bands) × 60 (electrodes) = 180 features that were used for this calculation. The weights $w_{0,class}$ and $w_{i,class}$ were determined for each class of movement such as grasping, opening, and scissor-shape hands.

$$g_{class}(x) = w_{0,class} + \sum_{j=1}^{N} w_{i,class} \times x_i$$

The class with the maximum value of $g_{class}(x)$ was chosen as the predicted movement class.[11,31] In the case of Decoder 1, the class corresponds to 1 of 2 states: R or M. For Decoder 2, the class corresponds to 1 of 3 types of movement: grasping, opening, and scissor-shape hand movements. The selected class indicated the predicted movement state or movement type.

Individual weights and biases for each class were determined using the linear SVM applied to a training data set.[25] First, the SVM algorithm was applied to each pair of class. The discriminant function, $g_{i,j}(x)$ for the discrimination of Class i and j, is expressed by a weighted sum of the features plus the bias. Using a training data set, a linear SVM finds the optimal weight and bias for the discriminant function. The pairwise discriminant functions comparing Class i and the other classes were simply added to yield the linear detector function:

$$g_i(x) = \sum_{m \neq i} g_{i,m}(x)$$

The SVM algorithm was implemented using Matlab 2007b.

Fivefold Cross-Validation

To test the generalization of the decoders, we used 5-fold

cross-validation as a performance measure.[2,3] We randomly divided the trials into 5 blocks, using 4 for training and 1 for testing. We then used all of the training data to train the classifier and evaluated its performance on the test data. This routine was repeated 5 times, and the averaged correct percentage over all runs is presented as a measure of decoder performance.

References

1. Andersen RA, Musallam S, Pesaran B: Selecting the signals for a brain-machine interface. **Curr Opin Neurobiol 14:**720–726, 2004
2. Bengio Y, Grandvalet Y: No unbiased estimator of the variance of K-fold cross-validation. **J Mach Learn Res 5:**1089–1105, 2004
3. Breiman L: Heuristics of instability and stabilization in model selection. **Ann Stat 24:**2350–2383, 1996
4. Chao ZC, Nagasaka Y, Fujii N: Long-term asynchronous decoding of arm motion using electrocorticographic signals in monkeys. **Front Neuroengineering 3:**3, 2010
5. Delorme A, Makeig S: EEGLAB: an open source toolbox for analysis of single-trial EEG dynamics including independent component analysis. **J Neurosci Methods 134:**9–21, 2004
6. Donoghue JP, Nurmikko A, Friehs G, Black M: Development of neuromotor prostheses for humans. **Suppl Clin Neurophysiol 57:**592–606, 2004
7. Fujiwara Y, Yamashita O, Kawawaki D, Doya K, Kawato M, Toyama K, et al: A hierarchical Bayesian method to resolve an inverse problem of MEG contaminated with eye movement artifacts. **Neuroimage 45:**393–409, 2009
8. Georgopoulos AP, Schwartz AB, Kettner RE: Neuronal population coding of movement direction. **Science 233:**1416–1419, 1986
9. Hochberg LR, Serruya MD, Friehs GM, Mukand JA, Saleh M, Caplan AH, et al: Neuronal ensemble control of prosthetic devices by a human with tetraplegia. **Nature 442:**164–171, 2006
10. Hosomi K, Saitoh Y, Kishima H, Oshino S, Hirata M, Tani N, et al: Electrical stimulation of primary motor cortex within the central sulcus for intractable neuropathic pain. **Clin Neurophysiol 119:**993–1001, 2008
11. Kamitani Y, Tong F: Decoding the visual and subjective contents of the human brain. **Nat Neurosci 8:**679–685, 2005
12. Kato R, Yokoi H, Arieta AH, Yu W, Arai T: Mutual adaptation among man and machine by using f-MRI analysis. **Robot Auton Syst 57:**161–166, 2009
13. Leuthardt EC, Schalk G, Moran D, Ojemann JG: The emerging world of motor neuroprosthetics: a neurosurgical perspective. **Neurosurgery 59:**1–14, 2006
14. Leuthardt EC, Schalk G, Wolpaw JR, Ojemann JG, Moran DW: A brain-computer interface using electrocorticographic signals in humans. **J Neural Eng 1:**63–71, 2004
15. Mehring C, Rickert J, Vaadia E, Cardosa de Oliveira S, Aertsen A, Rotter S: Inference of hand movements from local field potentials in monkey motor cortex. **Nat Neurosci 6:**1253–1254, 2003
16. Miller KJ, Zanos S, Fetz EE, den Nijs M, Ojemann JG: Decoupling the cortical power spectrum reveals real-time representation of individual finger movements in humans. **J Neurosci 29:**3132–3137, 2009
17. Nakamura T, Kita K, Kato R, Matsushita K, Hiroshi Y: Control strategy for a myoelectric hand: measuring acceptable time delay in human intention discrimination. **Conf Proc IEEE Eng Med Biol Soc 2009:**5044–5047, 2009
18. Pistohl T, Ball T, Schulze-Bonhage A, Aertsen A, Mehring C: Prediction of arm movement trajectories from ECoG-recordings in humans. **J Neurosci Methods 167:**105–114, 2008
19. Quian Quiroga R, Panzeri S: Extracting information from neuronal populations: information theory and decoding approaches. **Nat Rev Neurosci 10:**173–185, 2009
20. Ray S, Crone NE, Niebur E, Franaszczuk PJ, Hsiao SS: Neural correlates of high-gamma oscillations (60-200 Hz) in macaque local field potentials and their potential implications in electrocorticography. **J Neurosci 28:**11526–11536, 2008
21. Schalk G, Miller KJ, Anderson NR, Wilson JA, Smyth MD, Ojemann JG, et al: Two-dimensional movement control using electrocorticographic signals in humans. **J Neural Eng 5:**75–84, 2008
22. Shain W, Spataro L, Dilgen J, Haverstick K, Retterer S, Isaacson M, et al: Controlling cellular reactive responses around neural prosthetic devices using peripheral and local intervention strategies. **IEEE Trans Neural Syst Rehabil Eng 11:** 186–188, 2003
23. Thakur PH, Bastian AJ, Hsiao SS: Multidigit movement synergies of the human hand in an unconstrained haptic exploration task. **J Neurosci 28:**1271–1281, 2008
24. Truccolo W, Friehs GM, Donoghue JP, Hochberg LR: Primary motor cortex tuning to intended movement kinematics in humans with tetraplegia. **J Neurosci 28:**1163–1178, 2008
25. Vapnik VN: **Statistical Learning Theory.** New York: Wiley, 1998
26. Velliste M, Perel S, Spalding MC, Whitford AS, Schwartz AB: Cortical control of a prosthetic arm for self-feeding. **Nature 453:**1098–1101, 2008
27. Waldert S, Preissl H, Demandt E, Braun C, Birbaumer N, Aertsen A, et al: Hand movement direction decoded from MEG and EEG. **J Neurosci 28:**1000–1008, 2008
28. Wessberg J, Stambaugh CR, Kralik JD, Beck PD, Laubach M, Chapin JK, et al: Real-time prediction of hand trajectory by ensembles of cortical neurons in primates. **Nature 408:**361–365, 2000
29. Wolpaw JR, Birbaumer N, McFarland DJ, Pfurtscheller G, Vaughan TM: Brain-computer interfaces for communication and control. **Clin Neurophysiol 113:**767–791, 2002
30. Wolpaw JR, McFarland DJ: Control of a two-dimensional movement signal by a noninvasive brain-computer interface in humans. **Proc Natl Acad Sci U S A 101:**17849–17854, 2004
31. Yanagisawa T, Hirata M, Saitoh Y, Kato A, Shibuya D, Kamitani Y, et al: Neural decoding using gyral and intrasulcal electrocorticograms. **Neuroimage 45:**1099–1106, 2009
32. Yokoi H, Kita K, Nakamura T, Kato R, Hernandez A, Arai T: Mutually adaptable EMG devices for prosthetic hand. **The International Journal of Factory Automation, Robotics and Soft Computing 1:**74–83, 2009

Manuscript submitted August 18, 2010.
Accepted January 5, 2011.
Please include this information when citing this paper: published online February 11, 2011; DOI: 10.3171/2011.1.JNS101421.

Supplemental online information:
Video: http://mfile.akamai.com/21490/wmv/digitalwbc.download.akamai.com/21492/wm.digitalsource-na-regional/jns10-1421.asx (Media Player)
http://mfile.akamai.com/21488/mov/digitalwbc.download.akamai.com/21492/qt.digitalsource-global/jns10-1421.mov (Quicktime)

Address correspondence to: Masayuki Hirata, M.D., Ph.D., Department of Neurosurgery, Osaka University Medical School, E6 2-2 Yamadaoka Suita, Osaka, Japan. email: mhirata@nsurg.med.osaka-u.ac.jp.

IEICE TRANS. COMMUN., VOL.E94–B, NO.9 SEPTEMBER 2011

INVITED PAPER Special Section on Information Communication Technology for Highly Reliable Human Health Care Services

A Fully-Implantable Wireless System for Human Brain-Machine Interfaces Using Brain Surface Electrodes: W-HERBS

Masayuki HIRATA[†a)], Kojiro MATSUSHITA[†], Takafumi SUZUKI[††], *Nonmembers*, Takeshi YOSHIDA[†††], *Member*, Fumihiro SATO[††††], Shayne MORRIS[†], Takufumi YANAGISAWA[†], Tetsu GOTO[†], *Nonmembers*, Mitsuo KAWATO[†††††], *Fellow, and* Toshiki YOSHIMINE[†], *Nonmember*

SUMMARY The brain-machine interface (BMI) is a new method for man-machine interface, which enables us to control machines and to communicate with others, without input devices but directly using brain signals. Previously, we successfully developed a real time control system for operating a robot arm using brain-machine interfaces based on the brain surface electrodes, with the purpose of restoring motor and communication functions in severely disabled people such as amyotrophic lateral sclerosis patients. A fully-implantable wireless system is indispensable for the clinical application of invasive BMI in order to reduce the risk of infection. This system includes many new technologies such as two 64-channel integrated analog amplifier chips, a Bluetooth wireless data transfer circuit, a wirelessly rechargeable battery, 3 dimensional tissue-fitting high density electrodes, a titanium head casing, and a fluorine polymer body casing. This paper describes key features of the first prototype of the BMI system for clinical application.

key words: *brain-machine interface, implantable device, wireless, brain surface electrodes, motor restoration*

1. Introduction

1.1 General Backgrounds

The brain-machine interface (BMI) is a new method for man-machine interface, which enables us to control machines and communicate with others without input devices but directly using brain signals alone (Fig. 1). There are many diseases and conditions that lead to a loss of muscular control without disruption of the patients' cognitive abilities. These include amyotrophic lateral sclerosis (ALS), brainstem stroke, spinal cord injury, muscular dystrophy, Parkinson's disease and cerebral palsy, etc. BMI technology can offer these patients greater independence and a higher quality of life by enabling the control of external devices to communicate with others and to manipulate their environment according to their will [1]. Functional restoration using BMI is a more feasible solution in the shorter term when compared to methods using neural regeneration or neural transplantation, which presently lack the critical technologies necessary to organize functional neural networks.

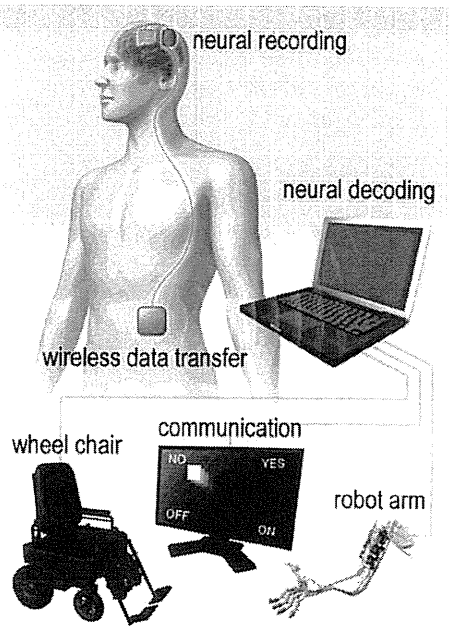

Fig. 1 A conceptual diagram of the brain machine interface.

There are two types of BMI. These are invasive BMI and non-invasive BMI. Invasive BMI requires surgical procedures and measures brain signals from intracranial electrodes (needle electrodes or brain surface electrodes), while non-invasive BMI measures brain signals non-invasively from outside of the body using scalp electrodes etc. To achieve higher performance and thus usefulness, we use invasive BMI techniques which involve the implantation of devices. For use in a practical situation, invasive BMI needs organic integration of the following medical and engineering technologies.

1) Neural recording with high spatiotemporal resolution

2) High speed transfer and processing of neural signals

3) Optimal extraction of neurophysiological features

Manuscript received April 19, 2011.
Manuscript revised May 10, 2011.

[†]The authors are with the Department of Neurosurgery, Osaka University, Medical School, Suita-shi, 565-0871 Japan.
[††]The author is with the Graduate School of Information Science and Technology, The University of Tokyo, Tokyo, 113-0033 Japan.
[†††]The author is with the Graduate School of Advanced Sciences of Matter, Hiroshima University, Higashihiroshima-shi, 739-8530 Japan.
[††††]The author is with Group of Electrical Engineering, Communication Engineering, Electronic Engineering, and Information Engineering, Tohoku University, Sendai-shi, 980-8578 Japan.
[†††††]The author is with ATR Brain Information Communication Research Laboratory Group, Kyoto-fu, 619-0288 Japan.
a) E-mail: mhirata@nsurg.med.osaka-u.ac.jp
DOI: 10.1587/transcom.E94.B.2448

Table 1 Brain signals used for BMI.

	Measured physiological phenomina	Spatial resolution	Temporal resolution	Time delay	Invasiveness	Long term recording stability	Portability
fMRI	CBF	○ 3-5mm	× 4-5s	× 4-5S	◎	○	×
NIRS	CBF	× 2cm	× 4-5s	× 4-5S	◎	○	○
EEG	Neural activities	× 3-4cm	○ 1ms	◎ 0	◎	○	○
MEG	Neural activities	△ 5-10mm	◎ 0.1ms	◎ 0	◎	○	×
ECoG	Neural activities	○ 2-3mm	◎ 0.1ms	◎ 0	△	◎	◎
LFP	Neural activities	○ 1mm	◎ < 0.1ms	◎ 0	×	△	◎
spike	Neuronal activities	◎ 0.2mm	◎ < 0.1ms	◎ 0	×	×	◎

NIRS: near-infrared spectroscopy, CBF: cerebral blood flow, MEG: magnetoencephalography, LFP: local field potential

4) Neural decoding
5) Control of external devices such as robots
6) Downsizing, integration, and implantation of electronic devices, and the use of wireless technology.
7) Non-invasive evaluations for appropriate surgical indications.
8) On-target survey and analysis of patient needs
9) Addressing of neuroethical issues

1.2 Clinical Studies Using Electrocorticograms Recorded from Brain Surface Electrodes

In the process of providing neurosurgical treatments for certain groups of patients, we sometimes record brain signals (electrocorticograms: ECoGs) or electrically stimulate the brain using electrodes directly placed on the brain surface. ECoGs selectively measure brain signals within the limited distance of a few milli-meters without distortion, and is in addition, insusceptible to external noises, while scalp skin electrodes measure distorted brain signals (electroencephalograms: EEGs) from a distance of up to a few centimeters. Furthermore, ECoG recording from brain surface electrodes is stable for at least as long as one year [2], whereas spike recordings from needle electrodes gradually deteriorate in yield due to chronic inflammatory tissue reactions. ECoG is a well-balanced brain signal for BMI (Table 1). Thus, we prefer to use ECoGs recorded by brain surface electrodes for BMI to achieve a high performance.

Eighteen subjects have participated in our clinical studies to date. All of the subjects were recruited from patients, whom we temporarily had to place brain surface electrodes, to treat intractable pain or intractable epilepsy. Informed consent was obtained from all of the patients. All studies were performed with the approval of the ethics committee of Osaka University Medical Hospital.

1.3 Neural Decoding Using Electrodes within Brain Grooves

Most of the primary motor cortex, which is responsible for the final output portion of motor commands, lies within the anterior wall of the central sulcus. Therefore if we can directly extract the brain signals from the central sulcus, it may be an optimal target for neural decoding of motor function. To demonstrate this hypothesis, we investigated ECoGs recorded from the brain surface electrodes inserted within the central sulcus during two or three types of simple motor tasks of the hand or the arm, such as grasping, pinching, and elbow flexion. We predicted the type of movement based on analysis of single trial ECoGs using a support vector machine (SVM) algorithm. As a result, we were able to predict movement types on a single trial basis with an accuracy rate of 70–90%. Specifically, we first demonstrated that ECoGs from the anterior wall of the central sulcus (the groove in the brain where most of the primary motor cortex lies) are useful for the accurate and early decoding of the movement types [3]. We consider that the extraction of appropriate neurophysiological features from the central sulcus contributed to the accuracy of our movement decoding.

1.4 Real Time Robot Control Using a Wired BMI System

We applied the above-mentioned decoding method using SVM to an ECoG based BMI system for the real time control of a robot arm. We also introduced successive SVM decoding every 200 ms. ECoGs were measured using a clinical 128-channel digital EEG system (EEG 2000; Nihon Koden Corporation, Tokyo, Japan) and digitized at a sampling rate of 1000 Hz. The robot arm was an experimental anthropomorphic hand developed by Prof. Yokoi [4]. As a result, we succeeded in the voluntary control of the grasping and releasing of objects [5]. Using a successive decoding and control algorithm, smooth robot-hand movement was achieved even though the decoding accuracy on a single trial basis was approximately 70%.

1.5 Necessity for a Fully-Implantable Wireless System

Wired leads which penetrate the skin pose a high risk of infection. It is necessary to fully implant a recording system within the body, in order to reduce infection risk through penetrating wire leads. For this reason, we are in the process of developing a fully-implantable ECoG recording system. Integrating this wireless system into the above-mentioned real time BMI system, we ultimately aim to develop a Wireless Human ECoG-based Real-time BMI System (**W-HERBS**).

In this paper, we describe the development of the first prototype of our fully-implantable wireless system for human brain-machine interfaces using brain surface electrodes.

2. System Overview

Figure 2 shows a schematic diagram of our fully-implantable wireless system. Figure 3 shows the first prototype. This fully-implantable system includes many new

technologies such as two 64-channel integrated analog amplifier chips, a Bluetooth wireless data transfer circuit, a wirelessly rechargeable battery, 3 dimensional tissue conformable high density electrodes, a titanium head casing, and a fluorine polymer body casing.

The implantable system consists of two parts. One is a head part and the other is a body part. The head part consists of tissue conformable brain surface micro-electrodes, a titanium head casing working as an artificial skull bone also, and a 128-ch integrated analog amplifier unit in it. The body part consists of a wireless data transfer unit and a microchip data controller, a wireless rechargeable unit, and a fluorine polymer body casing.

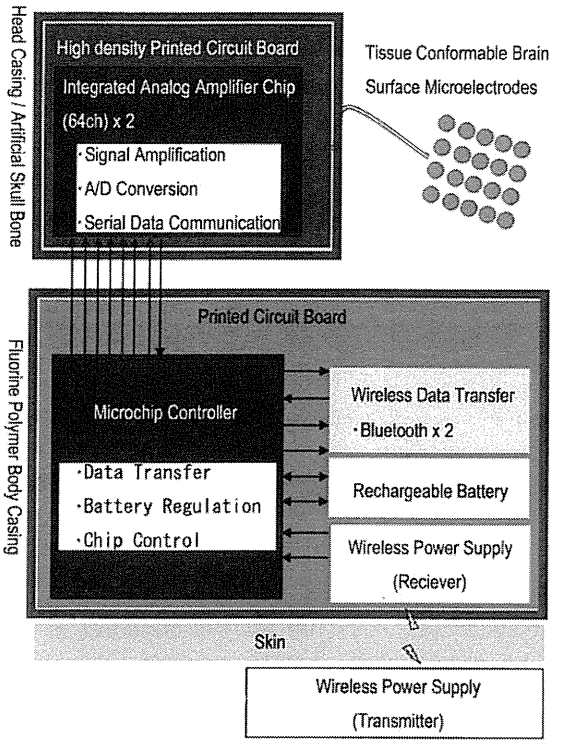

Fig. 2 Schematic diagram of the fully-implantable wireless system.

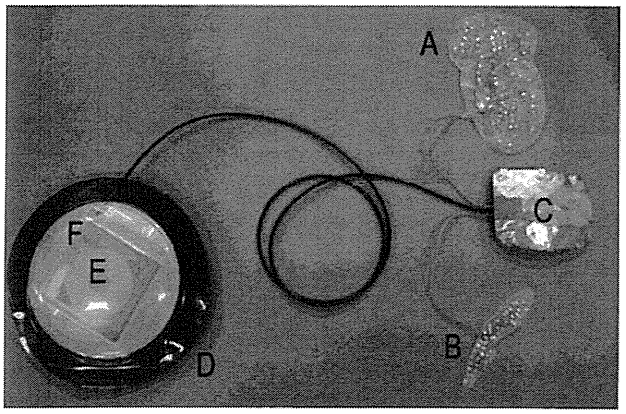

A. Brain surface microelectrodes conformable to the outer surface of the individual brain.
B. Brain surface microelectrodes conformable to the brain groove.
C. A titanium head casing / artificial skull bone.
D. A fluorine polymer body casing.
E. A wireless rechargeable unit, F. A wireless data transfer unit

Fig. 3 The first prototype of the fully-implantable wireless system for the W-HERBS.

3. Integrated Analog Amplifier Unit

ECoG is characterized as the signals with low frequency bands from 0.1 Hz to 500 Hz and small amplitudes from 1 μV to 1 mV (Fig. 4 A). It is necessary to reduce the input-referred noise of amplifier to record it [6]. Variable bandwidth and wide dynamic ranges are also important,because commercial AC noises with similar frequency bands easily contaminate ECoG signals. Thus, a high-linearity low noise amplifier with a variable bandwidth was developed to cover the frequency bands and voltage gains appropriate for recording ECoG signals [7]. The low noise amplifier with 0.1 Hz roll-off frequency is implemented with core differential amplifiers using large size MOSFETs and capacitor feedback scheme biased by ultrahigh resistors of cascade 12 MOSFETs (Fig. 4 B). A VLSI chip was fabricated using CMOS 0.18 μm process technology in the chip fabrication program of VLSI Design and Education Center (VDEC), the University of Tokyo.

Specifications of the chip functions are as follows.

- channel numbers: 64 channels
- 12 bits A/D converter

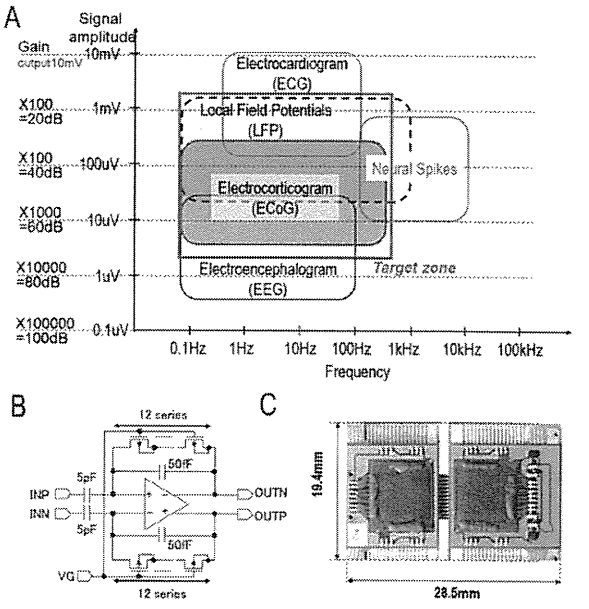

A: Target frequency bands and gains to cover ECoG signals and local field potentials (LFP). B: A circuit schematic of low-noise amplifier. C: A 128-channel integrated analog amplifier board

Fig. 4 Integrated analog amplifier.

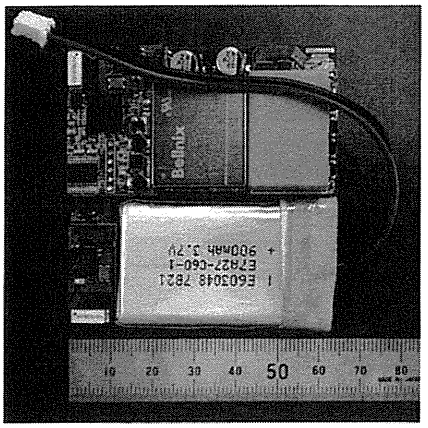

Fig. 5 Wireless data transfer unit.

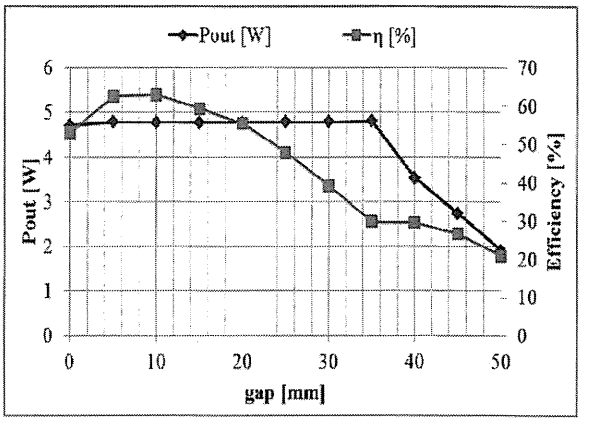

Fig. 6 Relationship between gap and power/efficacy of the wireless rechargeable unit. η indicates % proportion of output to input in the free space.

- voltage gain: 40–80 dB
- signal frequency bands: 0.1–1000 Hz
- input referred noise: 2.8 μV
- power consumption: 4.9 mW
- chip size: 5.0 mm × 5.0 mm
- master/slave function for a 128-channel system

A 128 channel analog amplifier board consists of two chips mounted on two high-density printed boards bridged by flexible printed wiring (Fig. 4 C). The size is 20 mm × 30 mm × 2.5 mm, which is small enough to be placed within a head casing described in Sect. 7.

4. Wireless Data Transfer Unit

We adapted the Bluetooth protocol communication (Class 2) for the first prototype for high usability. A combination of 2 sets of Bluetooth circuits enabled us to achieve effective data transmission rates of 400 kbps, which allows the transfer of 128-ch × 12-bit ECoG data in real time. Power consumption is approximately 300 mW, which means that most of the whole systems power is consumed by the wireless data transfer. Further improvements in the data transfer protocol should be made to achieve faster and less power consuming operation of the system. The size is 60 mm × 60 mm × 8 mm, which also needs to be reduced (Fig. 5). One of the solution is to change data transfer protocol from Bluetooth to WLAN or UWB.

5. Wireless Rechargeable Unit

The wireless battery charging system consists of two parts. One is a transmitter outside of the human body, and the other is a receiver inside of the human body. We achieved a wireless charging power of 4 W at a distance of 38 mm, which is sufficient to work the whole implantable system (Fig. 6). The coil size of the abdominal part is 40 mm in diameter and 8 mm in thickness, which may be scaled down, if the power consumption is reduced.

6. Tissue Conformable Brain Surface Microelectrodes

In order to record ECoGs with higher spatiotemporal resolution, we developed 3 dimensional high density grid electrodes, which fit to an individual's brain surface [8]. We extracted 3 dimensional surface data of the brain surface and the brain groove from the patient's individual MR images. An automatic brain groove extraction software (Brain VISA, http://brainvisa.info/) was used. Then we designed male and female molds for the grid electrodes using 3D CAD software (3 matic, Materialize Japan, Tokyo) (Fig. 7). The molds were then rapidly produced by a 3D printer. Silicon sheets fitting the brain surface were made with these molds. The location of each platinum electrode (1.0 mm in diameter) was designed with 3D CAD, taking account of the individual's anatomical information. Inter-electrode spacing was up to 2.5 mm. Regarding brain groove grid electrodes, electrodes can be located on both sides of the electrode sheet. These 3D grid electrodes fit to the brain surface with only minimal compression of the brain tissue, and with high ECoGs yields due to their close contact with the brain surface.

7. Head Casing and Artificial Skull Bone

We developed a head casing made of titanium, which contains a 128 ch amplifier unit. This casing works as a head casing as well as an artificial skull bone, cut to fit a patient's individual skull bone shape using 3D CAD (3 matic) and 3D CAM (Gibbs CAM, Gibbs and Associates, USA) softwares (Fig. 8) [9]. This head casing not only has cosmetic advantages, but it is also safer because other convex shapes pose a higher risk of cutaneous fistula.

8. Fluorine Polymer Body Casing

Compared to a head casing, a body casing offers larger space and does not require careful cosmetic consideration. We

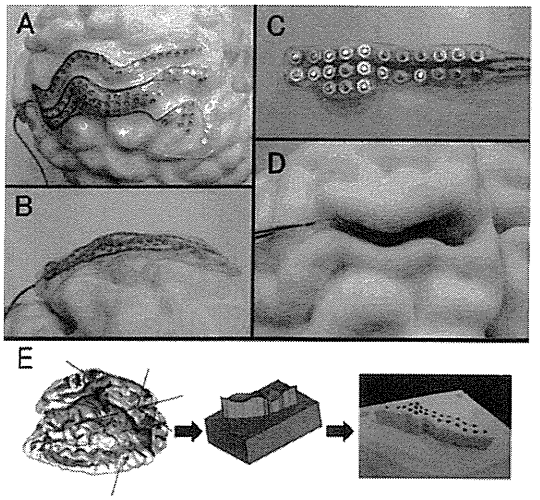

Tissue conformable brain surface microelectrodes fit individual brain surfaces. A, B: Gyral (brain surface) electrodes. C, D: Sulcal (brain groove) electrodes. E: Mold designed with 3D CAD software after automatic sulcal detection.

Fig. 7 Tissue conformable brain surface microelectrodes.

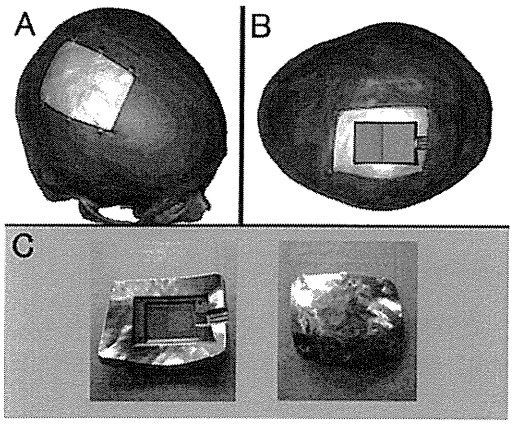

A, B: Head casing designed using 3D CAD software. Three dimensional skull bone data were obtained from individual's CT images. A: Outer side view. B: Inner side view. The head casing contains two 64-channel integrated amplifier chips on a small mounting board which are mounted on a folded inner panel as indicated in a gray color. C: A prototype casing. Left: inner side view. Right: outer side view.

Fig. 8 A titanium head casing/artificial skull bone.

introduced a soft casing made of fluorine polymer, which has advantages in terms of cost, chemical stability, durability, as well as biocompatibility. This body casing embeds a wireless data transfer unit and a microchip data controller, a wireless power supply unit and a rechargeable battery in silicone covered by fluorine polymer films.

9. Concluding Remarks

We have developed the first prototype of a fully-implantable wireless system. A fully-implantable wireless system is indispensable for the clinical application of invasive BMI to reduce the risk of infection. Sufficient bench testing and animal experiments are necessary in advance to the clinical situation.

BMI is a typical application where advanced methods for telecommunication are required. The telecommunication should be highly reliable to meet the demands of BMI used for medical devices. Also, it should operate with minimal delay, should transmit a plenty of data, should have high tissue permeability, and should be small enough to be implanted. A high-speed digital data transfer protocol with high tissue permeability meets our needs. A high band UWB chip is one of the candidates. There are great expectations for the progress of medical telecommunication.

Acknowledgments

This work was supported by the Strategic Research Program for Brain Sciences of MEXT. We would like to acknowledge Atsushi Iwata (A-R-Tec Corp), Shinichi Morikawa, Yoshihiro Watanabe (Unique Medical), Naohiro Hayaishi (Keisuugiken Corp), Shinichi Yoshimura, Shuhei Kosaka (Aska Electric Co Ltd), and Hirofumi Itoh (Junkosha Inc) for prototype manufacturing of our implantable system, and also thanks to VLSI Design and Education Center (VDEC), the University of Tokyo for the offer of chip fabrication program.

References

[1] J.R. Wolpaw, N. Birbaumer, D.J. Mcfarland, G. Pfurtscheller, and T.M. Vaughan, "Brain-computer interfaces for communication and control," Clin Neurophysiol, vol.113, no.6, pp.767–791, June 2002.
[2] Z.C. Chao, Y. Nagasaka, and N. Fujii, "Long-term asynchronous decoding of arm motion using electrocorticographic signals in monkeys," Front Neuroengineering, vol.3, p.3, 2010.
[3] T. Yanagisawa, M. Hirata, Y. Saitoh, A. Kato, D. Shibuya, Y. Kamitani, and T. Yoshimine, "Neural decoding using gyral and intrasulcal electrocorticograms," Neuroimage, vol.45, no.4, pp.1099–1106, May 2009.
[4] H. Yokoi, K. Kita, and T. Nakamura, "Mutually adaptable EMG devices for prosthetic hand," The International Journal of Factory Automation, Robotics and Soft Computing, pp.74–83, 2009.
[5] T. Yanagisawa, M. Hirata, Y. Saitoh, T. Goto, H. Kishima, R. Fukuma, H. Yokoi, Y. Kamitani, and T. Yoshimine, "Real-time control of a prosthetic hand using human electrocorticograms," J Neurosurg, vol.114, no.6, pp.1715–1722, 2011.
[6] T. Yoshida, Y. Masui, R. Eki, A. Iwata, Y.M., and K. Uematsu, "A neural recording amplifier with low-frequency noise suppression," IEICE Trans. Electron., vol.E93-C, no.6, pp.849–854, June 2010.
[7] T. Yoshida, K. Sueishi, A. Iwata, K. Matsushita, M. Hirata, and T. Suzuki, "A high-linearity low-noise amplifier with variable bandwidth for neural recording systems," Jpn. J. Appl. Phys., vol.50, no.4, p.04DE07, 2011.
[8] M. Hirata, T. Yoshimine, Y. Saitoh, T. Yanagisawa, T. Goto, Y. Watanabe, and T. Saito, Osaka University, Intracranial electrode and method for producing same. US patent application, 12/378,695, 2009/2/18.
[9] M. Hirata, T. Yoshimine, K. Matsushita, T. Goto, T. Yanagisawa, T. Suzuki, and S. Yoshimoto, Osaka University et al, PCT patent application, PCT/JP2011/001402, 2011/3/10.

Masayuki Hirata (B.S., M.S. and M.D. and Ph.D.) graduated from Faculty of Engineering, The University of Tokyo in 1985 and Osaka University Medical School in 1994. Board-certified neurosurgeon specialized in functional neurosurgery. He was promoted to a Specially-Appointed Associate Professor, Dept. of Neurosurgery, Osaka University Medical School serving as a leader of neural engineering group.

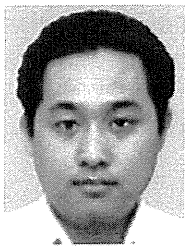

Kojiro Matsushita (B.S., Ph.D.) graduated from Dept. of Engineering, Tokyo Uni-versity of Science in 2000, a research fellow in Dept. of Informatics, Univ. of Zurich in 2001–2002, graduate student in Dept. of Informatics, the Univ. of Sussex in 2003–2004, graduated from Graduate School of Engineering, The Univ. of Tokyo in 2007, and a postdoctoral fellow in Computer Science and Artificial Intelligence Labo- ratory, MIT, in 2008. He was recruited as a Specially-Appointed Assistant Professor, Department of Neurosurgery, Osaka Uni-versity Medical School in 2009.

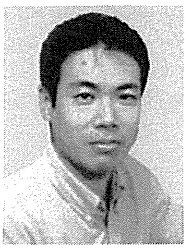

Takafumi Suzuki received B.E., M.E. and Ph.D. degrees in Engineering from the University of Tokyo in 1993, 1995 and 1998, respectively. From 1998 to 2002, he was a research associate at the University of Tokyo. He is currently an assistant professor at Graduate School of Information science and technology, the University of Tokyo.

Takeshi Yoshida received B.E., M.E. and Ph.D. degrees in engineering from Hiroshima University in 1994, 1996 and 2004, respectively. From 1996 to 2001, he was with System Electronics Laboratories, Nippon Telegraph and Telephone Corporation. He is currently an assistant professor at Graduate School of Advanced Sciences of Matter, Hiroshima University.

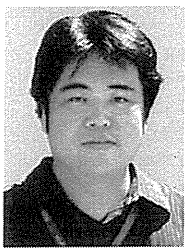

Fumihiro Sato received B.S. and Ph.D. degrees in Engineering from Tohoku Gakuin University in 1995 and 2000, respectively. From 2000 to 2006, he was an assistant professor at Tohoku University. He is currently an associate professor of Dept. of Electric Engineering, Tohoku University.

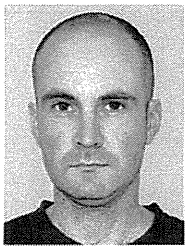

Shayne Morris received an MBA from Yokohama National University in 1994. Following this he received an M.D. degree in Medicine from Osaka University in 2002, and is presently in a Ph.D. course at Osaka University, studying functional neuro-surgery in Osaka University Graduate School of Medicine.

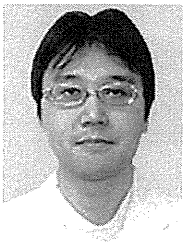

Takufumi Yanagisawa (M.D., Ph.D.) graduated from Dept. of Physics, Waseda University and Osaka University Medical School in 2005. Board-certified neuro-surgeon. He learned decoding of brain signals under Kamitani Labo at ATR Com-putational Neuroscience Laboratories. He is currently appointed as a Specially-Appointed Researcher, Dept. of Neuro-surgery, Osaka University Medical School with a principal interest in decoding of eletrocorticogram.

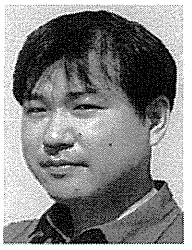

Tetsu Goto (M.D., Ph.D.) graduated from Osaka University Medical School in 2002. Board-certified neurosurgeon, currently Assistant Professor, Department of Neuro-surgery, Osaka University Medical School and Division of Health Sciences. He is specialized in the analysis of motor and language signals recorded with magneto-encephalography and electrocorticography.

Mitsuo Kawato (B.S., M.E., Ph.D.) graduated from Faculty of Physics, The University of Tokyo in 1976 and Dept. of Biophysical Engineering, Osaka University in 1978. He has been a faculty member at Osaka University in 1981–1988, recruited to ATR, in 1988, currently serving as Director, ATR Brain Information Communication Research Laboratory Group since 2010. He is acknowledged as a pioneer in computa-tional neuroscience including internal models in the cerebellum and robot learning. He is appointed as Research Supervisor of JST, Decoding and Controlling Brain Information.

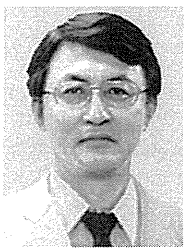

Toshiki Yoshimine (M.D., Ph.D.) graduated from Osaka University Medical School in 1975. Board-certified neurosurgeon, specialized in brain tumor and epilepsy surgery. He is a Director, Japan Neuro-surgical Society, and Neurotrauma Com-mittee Member, World Federation of Neuro-surgical Societies (WFNS). He has been a research fellow in Mayo Clinic in 1980–1983, a visiting professor in University of Mainz in 1995. He currently serves as Professor and Chairman, Dept. of Neur-osurgery, Osaka University Medical School and Director, Medical Center for Transla-tional Research, Osaka University Hospital.